JACS
JOURNAL OF THE AMERICAN CHEMICAL SOCIETY
Communication
pubs.acs.org/JACS

Room-Temperature Dual-Wavelength Lasing from Single-Nanoribbon Lateral Heterostructures

Jinyou Xu,[†,§] Liang Ma,[†,§] Pengfei Guo,[†,§] Xiujuan Zhuang,[†] Xiaoli Zhu,[†] Wei Hu,[†] Xiangfeng Duan,[‡] and Anlian Pan*[,†]

[†]Key Laboratory for Micro-Nano Physics and Technology of Hunan Province, State Key Laboratory of Chemo/Biosensing and Chemometrics, College of Physics and Microelectronics Science, Hunan University, Changsha 410082, China

[‡]Department of Chemistry and Biochemistry and California NanoSystems Institute, University of California at Los Angeles, Los Angeles, California 90095, United States

Supporting Information

ABSTRACT: Nanoscale dual-wavelength lasers are attractive for their potential applications in highly integrated photonic devices. Here we report the growth of nanoribbon lateral heterostructures made of a CdS_xSe_{1-x} central region with epitaxial CdS lateral sides using a multistep thermal evaporation route with a moving source. Under laser excitation, the emission of these ribbons indicates sandwich-like structures along the width direction, with characteristic red emission in the center and green emission at both edges. More importantly, dual-wavelength lasing with tunable wavelengths is demonstrated at room temperature based on these single-nanoribbon heterostructures for the first time. These achievements represent a significant advance in designing nanoscale dual-wavelength lasers and have the potential to open up new and exciting opportunities for diverse applications in integrated photonics, optoelectronics, and sensing.

Dual-wavelength or color laser sources are desirable in a multitude of practical applications, such as wavelength-division-multiplexed communication systems, optical signal processing, biomedical research, and so on.[1−4] To date, most dual-wavelength lasers have been made of rare earth ion-doped fibers[1,2] and solid-state bulk materials.[3] With the development of integrated photonics, the design of diverse nanoscale dual-wavelength lasers is of considerable interest. However, most of the dual-wavelength lasers reported to date suffer the limitation of relatively large footprints and are unsuitable for highly integrated photonic circuits and systems on chips.

One-dimensional (1D) semiconductor nanostructures can simultaneously function as both the active gain material and optical waveguide cavities,[5−12] and can be ideally suited for creating nanoscale semiconductor lasers for integrated photonic applications.[13−17] However, most 1D semiconductor lasers operate at a single wavelength with limited tunability derived from either the Fabry−Perot or whispering-gallery mode emission. Dual-wavelength or color lasers with wide wavelength separation from single semiconductor nanostructures have not been reported.

Here we report the growth of new CdS_xSe_{1-x}-CdS nanoribbon lateral heterostructures, with composition-tunable alloy CdS_xSe_{1-x} at the center and epitaxial CdS at the lateral sides. The photoluminescence image shows these ribbons exhibit a fine sandwich-like structure along the width direction. Based on these structures, dual-wavelength nanolasers can be achieved with the lasing wavelength spacing continuously tunable by varying the composition of the central CdS_xSe_{1-x} alloy.

The CdS_xSe_{1-x}-CdS nanoribbon lateral heterostructures were grown by a multistep thermal evaporation route with a moving source.[18,19] In a horizontal furnace (OTF-1200X) with a 1-in. quartz tube (inner diameter 45 mm, length 180 cm), an alumina boat with CdS powder (Alfa Aesar, 99.99%) was first pulled into the heating zone of the furnace, and two other boats with CdSe and CdS powder (Alfa Aesar, 99.99%), respectively, were placed in the downstream and upstream of the tube and located far enough away from the heating zone before growth. A quartz rod driven by a step motor through magnetic force was used to push these two boats into/out of the heating zone during the growth. Several silicon wafers coated with 2-nm-thick Au films were placed in the downstream of the gas flow to collect the deposited ribbons, as schematically shown in Figure S1 (Supporting Information). Before heating, a N_2 flow was introduced into the system at a rate of 150 sccm for 20 min to purge the O_2 inside the tube. The furnace temperature was then ramped to 850 °C at a rate of 40 °C/min, while maintaining the pressure at 300 mbar. After 40 min of growth, the CdSe boat was quickly pushed into the heating zone by the step motor to replace the CdS boat. After a period time (10−40 min) of growth, the boat was pushed out of the heating zone and the temperature was reduced to 800 °C. The other CdS boat was then quickly pushed into the heating zone, and the growth was kept at 800 °C for an additional 30 min. After the growth, the temperature was naturally reduced to room temperature.

A typical scanning electron microscopy (SEM) image shows that the as-grown sample is composed of nanoribbons with length up to tens of micrometers, width ranging from 1 to 10 μm (Figure 1A), and thickness of 100−400 nm (Figure S2, Supporting Information). Some ribbons were picked out from the original grown substrate and transferred onto a transparent MgF_2 wafer (refractive index ∼1.39) by using a homemade fiber taper under an optical microscope (Zeiss, Imager. A2). A

Received: May 24, 2012
Published: July 17, 2012

   dx.doi.org/10.1021/ja3050458 | J. Am. Chem. Soc. 2012, 134, 12394−12397

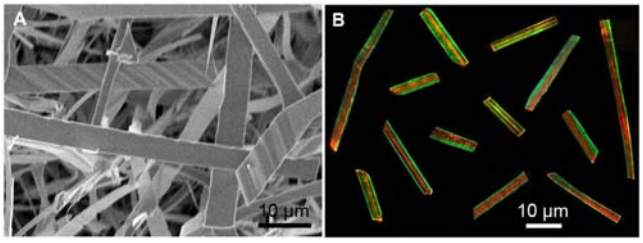

Figure 1. (A) SEM image of as-prepared nanoribbon lateral heterostructures. (B) Real-color photograph of some nanoribbon lateral heterostructures picked out from the initial grown substrate and dispersed on a transparent MgF_2 wafer under diffused 405-nm laser illumination.

real-color photograph of some selected ribbons under the illumination of a 405-nm continuous wave (CW) laser (Figure 1B) shows, based on the emission color, that these ribbons have a fine sandwich-like structure, with green color on both lateral sides and red color in the central region. The well-defined interfaces indicate an abrupt change of the bandgap/composition between the lateral sides and the central region of the ribbons.

Transmission electron microscopy (TEM) combined with energy-dispersive X-ray spectroscopy (EDX) were used to investigate the microstructure and elemental composition of these ribbons. Figure 2A is a typical TEM image of a

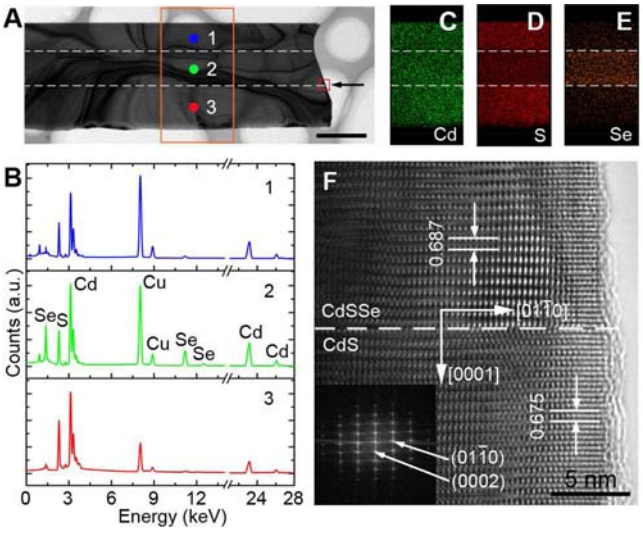

Figure 2. (A) TEM image of a nanoribbon lateral heterostructure (scale bar, 2 μm) and (B) corresponding TEM-EDX profiles recorded from three different positions (1–3) in the ribbon. (C–E) 2D elemental mapping for the three detected elements, Cd, S, and Se, respectively. (F) HRTEM image taken from the tip of the interface and FFT pattern (inset).

representative nanoribbon with a uniform width of ~3 μm. Figure 2B plots the EDX spectra collected from three different positions along the width direction of the ribbon (dots 1–3 in Figure 2A), which reveal that positions 1 and 3 (lateral sides) mainly consist of S and Cd elements with negligible Se element detected, while position 2 (central region) is composed of considerable Se, S, and Cd elements (the detected Cu element originates from the microgrid). Figure 2C–E shows two-dimensional (2D) elemental mapping of a selected region of this ribbon (marked with an orange rectangle in Figure 2A) for the detected elements, Cd, S, and Se, respectively. As can be seen, Cd is very homogeneously distributed across the whole ribbon (Figure 2C), while S is located more in both lateral sides than in the central region of the ribbon (Figure 2D), and Se is almost completely distributed in the central region of the ribbon (Figure 2E). The elemental analyses prove that these ribbons are actually lateral heterostructures with CdS compound on both lateral sides and CdS_xSe_{1-x} alloy compound in the central region, which well explains the observed fine sandwich-like color structure in Figure 1B.

Figure 2F shows the high-resolution TEM (HRTEM) image taken from the tip of the interface region of the ribbon (see the red rectangle in Figure 2A), where a well-defined heterointerface between the central CdS_xSe_{1-x} and lateral CdS (indicated with a dashed line) is clearly observed. Both the central CdS_xSe_{1-x} and the lateral CdS keep a single-crystalline structure without significant defects. The measured plane spacing in the lateral region is 0.675 nm, consistent with the (0002) lattice spacing of wurtzite CdS, while the plane spacing in the central region (0.687 nm) is a little larger than that of the lateral side, in agreement with the (0002) lattice spacing of wurtzite CdS_xSe_{1-x} alloy with S mole fraction $x \approx 0.41$.[20] The corresponding fast Fourier transform (FFT) pattern (inset) shows a well-defined single set of diffraction spots, indicating the single-crystalline nature in the interface region of the ribbons. The above results clearly demonstrate that the achieved nanoribbons are high-quality CdS-CdS_xSe_{1-x} lateral heterostructures, with the lateral CdS epitaxially grown on the $\pm$(0001) surfaces of the pre-existing CdS_xSe_{1-x} ribbons.[21,22]

Spatially resolved micro-photoluminescence (μ-PL) measurements along the width direction of individual ribbons were performed on a confocal μ-PL system (WITec, alpha-300). Figure 3A gives the real-color photograph of an examined

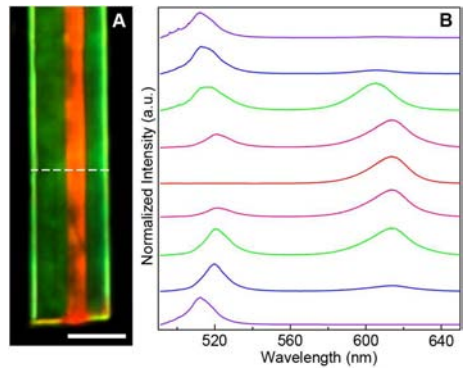

Figure 3. (A) Real-color photograph of a representative nanoribbon lateral heterostructure illuminated with a 405-nm laser (scale bar, 5 μm). (B) Normalized μ-PL spectra collected along the dashed line in panel A.

ribbon under the illumination of a CW laser (405 nm), and Figure 3B gives a series of μ-PL spectra collected at several different regions along its width (see the indicated dashed line). We can see that the PL spectra from both lateral sides (violet lines) and the central region (red line) exhibit a strong single peak with wavelengths of 517 and 615 nm, respectively. The peak wavelength of the emission band at the lateral sides (517 nm) is consistent with the near-band-edge energy of CdS (2.42 eV), and the peak wavelength at the central region (615 nm) is consistent with the band-edge emission of $CdS_{0.41}Se_{0.59}$ alloy.[20] The spectra collected at the interface region (blue, green, and

dx.doi.org/10.1021/ja3050458 | J. Am. Chem. Soc. 2012, 134, 12394–12397

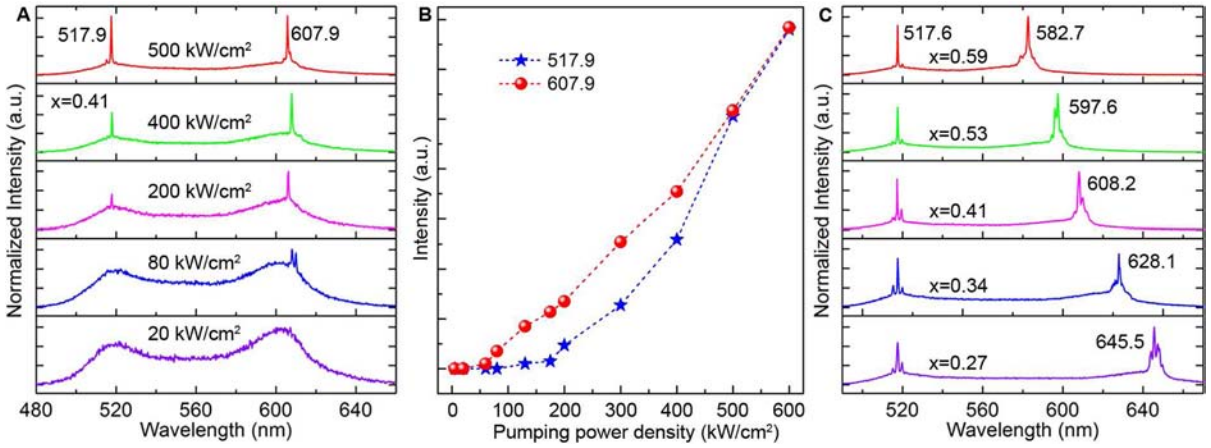

Figure 4. (A) Pumping power-dependent PL spectra of a nanoribbon lateral heterostructure at room temperature. (B) Pumping power-dependent intensity for the green (~517.9 nm, pentagrams) and the red (~607.9 nm, spheres) lasing peaks, respectively. (C) Dual-wavelength lasing with different wavelength spacing.

pink) exhibit two peaks, coming from the emission of both the central and lateral regions simultaneously. Importantly, all the nanoribbons exhibit clean band-edge emission with no obvious trap-level emission observed across the entire ribbon, including the interface region, indicating the high quality of the nanoribbons and few defects even at the strained interface. The μ-PL results are in good agreement with the previous structural and compositional characterizations (Figure 2), and further demonstrate well the laterally epitaxial growth of these nanoribbons.

Based on the above structural and spectral analyses, the growth of these lateral heterostructures mainly involves three stages (see Figure S3, Supporting Information). At the initial stage, CdS nanoribbons were first grown through the co-presence growth of vapor−liquid−solid and vapor−solid mechanisms[21,22] when the CdS powder is heated to 850 °C. After the formation of CdS nanoribbons, the CdS boat is replaced by the CdSe boat, and the pre-grown CdS ribbons would be converted into CdS_xSe_{1-x} alloy ribbons through anion exchange of S with Se,[23,24] since the enthalpy of formation (ΔH_f) of CdS (−148.31 ± 4.25 kJ/mol) is lower than that of CdSe (−141.12 ± 3.83 kJ/mol),[25] making the conversion reaction from CdS to CdS_xSe_{1-x} much more favorable kinetically and thermodynamically than the opposite reaction. After a period of conversion reaction, the furnace temperature is reduced to 800 °C and the other CdS boat iss pushed into the heating zone. At this stage, the pre-existing CdS_xSe_{1-x} alloy is relatively chemically stable and fundamentally difficult to convert into CdS again due to its relatively larger ΔH_f ($-148.10 \pm 6.75 < \Delta H_f < -144.04 \pm 3.21$).[25] As a result, the CdS vapor from the source would be preferentially deposited onto the chemically active ±(0001) polar surfaces of the pre-formed CdS_xSe_{1-x} ribbons, leading to the epitaxial growth of the CdS laterals along the [0001] direction. From this growth mechanism, the composition and the bandgap in the central region of the ribbons can be tuned by controlling the growth time and/or temperature of the conversion reaction from CdS to CdS_xSe_{1-x} during the second stage, controlling the emission wavelength of the central region (Figure S4, Supporting Information).

These two-emission nanoribbon heterostructures offer promising applications in designing diverse compact photonic components. A dual-wavelength (color) nanoscale laser is achieved based on such a lateral heterostructure, pumped by a pulse laser (Nd:YAG, 355 nm) at room temperature. Figure 4A shows the PL spectra of a representative ribbon (20 μm × 5 μm × 200 nm) pumped at different powers. At a relatively low pumping (20 kW/cm^2), two broad band-edge emission bands with peak wavelength respectively at 515 and 604 nm appear, consistent with the previous observations under CW laser excitation (Figure 3B). When the pumping power is increased to 80 kW/cm^2, new sharp emission lines (607.9 and 610.1 nm) with the fwhm of ~0.7 nm start to emerge at the low-energy side of the red band (604 nm), while the green band (515 nm) shows no significant change in spectral shape at this stage. When the pumping power is further elevated to 200 kW/cm^2, the intensity of the sharp emission at 607.9 nm strongly increases; meanwhile, a new sharp emission line (~517.9 nm) appears from the green emission band. The appearance of sharp emission lines from the two broad band-edge emission bands indicates the transition from spontaneous to stimulated emission. Under a much higher pumping, the intensities of these two sharp peaks are both rapidly increased, and a dual-wavelength lasing can be achieved when the pumping power is above 400 kW/cm^2.

Figure 4B shows the pumping power-dependent intensity for the green and red lasing peaks, respectively, which reveals that the threshold of the red lasing peak (~80 kW/cm^2) is lower than that of the green one (~200 kW/cm^2). The threshold for a composition-homogeneous semiconductor laser is determined by a series of factors,[26] such as the optical gain of the material, the amount of the material that can provide the gain, and so on. Here in these CdS_xSe_{1-x}-CdS heterostructured ribbons, the lasing process is more complicated than that in the composition-homogeneous laser, since the emission of the green band from the CdS laterals can be partially reabsorbed by the central CdS_xSe_{1-x} due to its relatively smaller bandgap. Considering that the optical gains of CdS and CdSSe are similar,[27] and the amount of CdS that provides the gain at the green lasing peak is more than that of CdSSe that provides the gain at the red lasing peak, as seen from the structure analyses (Figure 2), the reabsorption process may play the key role accounting for the lower threshold of the red lasing peak. The green emission from the lateral region could suffer from considerable reabsorption-induced loss during its travel along the ribbon cavity, and simultaneously the red emission in the

dx.doi.org/10.1021/ja3050458 | J. Am. Chem. Soc. 2012, 134, 12394−12397

central region would obtain additional gain from the green emission. The above discussion would explain why the red emission has a lower lasing threshold than that of green one. More importantly, the wavelength spacing of the two lasing lines can be tuned by adjusting the composition of the central region of the ribbons, which can be controlled with the experimental parameters of the growth (growth time, temperature, and pressure), as previously discussed. Figure 4C plots five representative dual-wavelength lasing spectra achieved from the ribbons with different central alloy compositions (x value), which show that the lasing wavelength at the high-energy region is almost fixed (~517 nm), while the lasing wavelength at the low-energy region can be continuously tuned from 582.7 to 645.5 nm, confirming the broad tunability of the spacing between the two lasing lines. In addition, it is worth noting that there are some weak emission lines accompanying each lasing line in almost all of the obtained lasing spectra, which is believed to result from different lasing modes, since the observed spacing between these multimodes is ~2 nm for the examined 20-μm-long ribbon (Figure 4A), which could agree quantitatively with the calculated spacing between adjacent resonance wavelength, taking the ribbon as a Fabry–Perot cavity.[7−9]

In summary, we have demonstrated that CdS_xSe_{1-x}-CdS nanoribbon lateral heterostructures can be synthesized through a multistep thermal evaporation route with a moving source. Photoluminescence studies show that the emission color of these ribbons indicates a fine sandwich-like structure, with red emission at the center and green emission at both edges. With these unique structures, we have further demonstrated for the first time that dual-color lasing can be achieved under pulsed laser excitation. More importantly, the spacing of the lasing wavelength of these nanoribbon lasers can be continuously tuned by controlling the composition and bandgap of the central CdS_xSe_{1-x} in the ribbons. The development of a nanoscale laser source with tunable dual wavelengths can open up exciting opportunities for diverse applications in integrated photonics, optoelectronics, and sensing.

■ ASSOCIATED CONTENT

Supporting Information

Experimental setup and detailed process; SEM image; illustrations of the growth of nanoribbon lateral heterostructures; and PL spectra from the ribbons with different central alloy composition. This material is available free of charge via the Internet at http://pubs.acs.org.

■ AUTHOR INFORMATION

Corresponding Author

anlian.pan@hnu.edu.cn

Author Contributions

[§]J.X., L.M., and P.G. contributed equally.

Notes

The authors declare no competing financial interest.

■ ACKNOWLEDGMENTS

The authors are grateful to the NSF of China (No. 90923014 and 10974050), the National Basic Research Program of China (No. 2012CB932703), the Research Fund for the Doctoral Program of Higher Education (20110161110034), and the Aid Program for Science and Technology Innovative Research Team in Higher Educational Institutions of Hunan Province for financial support.

■ REFERENCES

(1) Liu, D.; Ngo, N. Q.; Dong, X. Y.; Tjin, S. C.; Shum, P. *Appl. Phys. B: Laser Opt.* **2005**, *81*, 807.
(2) Abdullah, F.; Noor, A. S. M.; Mahdi, M. A.; Jamaludin, M. Z.; Dimyati, K.; Abdullah, M. K. *Opt. Laser Technol.* **2005**, *37*, 638.
(3) Walsh, B. M.; Murray, K. E.; Barnes, N. P. *J. Appl. Phys.* **2002**, *91*, 11.
(4) Xiao, L. H.; Wei, L.; Cheng, X. D.; He, Y.; Yeung, E. S. *Anal. Chem.* **2011**, *83*, 7340.
(5) Chu, S.; Wang, G. P.; Zhou, W. H.; Lin, Y. Q.; Chernyak, L.; Zhao, J. Z.; Kong, J. Y.; Li, L.; Ren, J. J.; Liu, J. L. *Nature Nanotechnol.* **2011**, *6*, 506.
(6) Qian, F.; Li, Y.; Gradečak, S.; Park, H. G.; Dong, Y.; Ding, Y.; Wang, Z. L.; Lieber, C. M. *Nat. Mater.* **2008**, *7*, 701.
(7) Duan, X. F.; Huang, Y.; Agarwal, R.; Lieber, C. M. *Nature* **2003**, *421*, 241.
(8) Johnson, J. C.; Choi, H. J.; Knutsen, K. P.; Schaller, R. D.; Yang, P.; Saykally, R. J. *Nat. Mater.* **2002**, *1*, 106.
(9) Huang, M. H.; Mao, S.; Feick, H.; Yan, H.; Wu, Y.; Kind, H.; Weber, E.; Russo, R.; Yang, P. *Science* **2001**, *292*, 1897.
(10) Xiao, Y.; Meng, C.; Wang, P.; Ye, Y.; Yu, H. K.; Wang, S. S.; Gu, F. X.; Dai, L.; Tong, L. M. *Nano Lett.* **2011**, *11*, 1122.
(11) Agarwal, R.; Barrelet, C. J.; Lieber, C. M. *Nano Lett.* **2005**, *5*, 917.
(12) Zhang, C.; Zou, C. L.; Yan, Y.; Hao, R.; Sun, F. W.; Han, Z. F.; Zhao, Y. S.; Yao, J. *J. Am. Chem. Soc.* **2011**, *133*, 7276.
(13) Law, M.; Sirbuly, D. J.; Johnson, J. C.; Goldberger, J.; Saykally, R. J.; Yang, P. *Science* **2004**, *305*, 1269.
(14) Yan, H.; Choe, H. S.; Nam, S. W.; Hu, Y. J.; Das, S.; Klemic, J. F.; Ellenbogen, J. C.; Lieber, C. M. *Nature* **2011**, *470*, 240.
(15) Duan, X. F.; Huang, Y.; Cui, Y.; Wang, J. F.; Lieber, C. M. *Nature* **2001**, *409*, 66.
(16) Friedman, R. S.; McAlpine, M. C.; Ricketts, D. S.; Ham, D.; Lieber, C. M. *Nature* **2005**, *434*, 1085.
(17) Sirbuly, D. J.; Law, M.; Pauzauskie, P.; Yan, H. Q.; Maslov, A. V.; Knutsen, K.; Ning, C. Z.; Saykally, R. J.; Yang, P. D. *Proc. Natl. Acad. Sci. U.S.A.* **2005**, *102*, 7800.
(18) Yang, Z. Y.; Xu, J. Y.; Wang, P.; Zhuang, X. J.; Pan, A. L.; Tong, L. M. *Nano Lett.* **2011**, *11*, 5085.
(19) Gu, F.; Yang, Z.; Yu, H.; Xu, J.; Wang, P.; Tong, L.; Pan, A. *J. Am. Chem. Soc.* **2011**, *133*, 2037.
(20) Pan, A.; Yang, H.; Liu, R.; Yu, R.; Zou, B.; Wang, Z. *J. Am. Chem. Soc.* **2005**, *127*, 15692.
(21) Kim, Y.; Jung, J.; Yoon, H.; Song, M.; Bae, S.; Kim, Y.; Chen, Z.; Zou, J.; Joyce, H.; Gao, Q. *Nanotechnology* **2010**, *21*, 145602.
(22) Ma, C.; Ding, Y.; Moore, D.; Wang, X.; Wang, Z. L. *J. Am. Chem. Soc.* **2004**, *126*, 708.
(23) Lee, J. Y.; Kim, D. S.; Park, J. *Chem. Mater.* **2007**, *19*, 4663.
(24) Dloczik, L.; Könenkamp, R. *Nano Lett.* **2003**, *3*, 651.
(25) Xu, F.; Ma, X.; Kauzlarich, S. M.; Navrotsky, A. *J. Mater. Res.* **2009**, *24*, 1368.
(26) Johnson, J. C.; Yan, H. Q.; Yang, P. D.; Saykally, R. J. *J. Phys. Chem. B* **2003**, *107*, 8816.
(27) Klingshirn, C. *Adv. Mater. Opt. Electron.* **1994**, *3*, 103.